AIAA JOURNAL
Vol. 42, No. 12, December 2004

Low-Order Modeling for Transonic Helicopter Noise

A. S. Morgans* and A. P. Dowling†
University of Cambridge, Cambridge, England CB2 1PZ, United Kingdom

The permeable surface form of the Ffowcs Williams–Hawkings equation provides an efficient basis for predicting helicopter rotor noise when the flow over the blades is transonic. It requires knowledge of the temporal variation of fictitious acoustic sources over the permeable control surface. Calculation of these using unsteady computational fluid dynamics (CFD) solvers is feasible for straightforward helicopter motion, but becomes prohibitively time consuming for more complicated maneuvers. Low-order modeling provides an efficient alternative. Because at transonic speeds significant noise originates at the shock surfaces, low-order modeling of the two-dimensional shock dynamics was first performed to provide an insight. Using data from CFD simulations, system identification, a modeling technique suitable for dynamically linear systems, was performed. The position of a well-formed shock was found to respond to variations in blade speed and blade pitch angle with approximate first-order lag relationships; these findings were consistent with harmonic tests. Low-order modeling of the acoustic sources was then performed, although for simplicity attention was restricted to two-dimensional motion and an acoustically compact control surface. Models were obtained, again using system identification, and were successfully used in noise prediction. Analytical consideration of the sources revealed that their dynamics arose mainly due to the shock motion. These findings serve to demonstrate the potential of low-order modeling in predicting transonic helicopter noise.

Nomenclature

A_{sh}	=	shock area per unit length of blade, m
a_i, b_j, c_k, d_l	=	infinite impulse response (IIR) filter coefficients
b	=	blade semichord, m
c	=	speed of sound in undisturbed flow, ms^{-1}
e	=	model error
f	=	0 defines location of the control surface S
H	=	Heaviside step function
$H(\omega)$	=	transfer function
I, J, K, L	=	IIR filter orders
I_1, I_2, I_3	=	$\int_S \rho_0 U_n \,\mathrm{d}S, \int_S L_x \,\mathrm{d}S, \int_S L_y \,\mathrm{d}S$
i	=	$\sqrt{-1}$
i_s	=	grid node of shock position
K	=	number of sinusoids in sum of sines signal
L_i	=	$p_{ij}n_j + \rho u_i(u_n - v_n)$
M	=	magnitude of $\boldsymbol{M}$
$\boldsymbol{M}$	=	Mach number vector
$\boldsymbol{n}$	=	unit vector normal to control surface
p	=	absolute pressure, Pa
p_{ij}	=	compressive stress tensor, Pa
$r(\tau)$	=	magnitude of radiation vector, $\lvert\boldsymbol{r}(\tau)\rvert$, m
$\boldsymbol{r}(\tau)$	=	radiation vector, $\lvert\boldsymbol{x}(t) - \boldsymbol{y}(\tau)\rvert$, m
S	=	control surface
s	=	Laplace transform variable, $i\omega$
T	=	sampling period, s
T_c	=	first-order lag time constant, s
T_d	=	time delay, s
t	=	observer time, s
U_i	=	$(1 - \rho/\rho_0)v_i + \rho/\rho_0 u_i$
$\boldsymbol{u}$	=	fluid velocity, ms^{-1}
V	=	volume, m^3
v	=	blade speed, ms^{-1}
$\boldsymbol{v}$	=	blade/control surface velocity, ms^{-1}
$\boldsymbol{x}$	=	observer position, m
x_s	=	shock position, m
$\boldsymbol{y}$	=	source position, m
z	=	z-transform variable, $e^{i\omega T}$
α	=	angle of attack, deg
δ	=	Dirac delta function
δ_{ij}	=	Kronecker delta
$\boldsymbol{\eta}$	=	coordinates in which S is stationary
ρ	=	density, kgm^{-3}
τ	=	source time, s
$\tau*$	=	retarded time, $t - r(\tau*)/c$, s
ϕ	=	random phase chosen on the range (0, 1)
ω	=	rotation rate or angular frequency, rads^{-1}
$\omega_{\min}, \omega_{\max}$	=	lower, upper limits of passband, rads^{-1}
$\Box^2$	=	wave operator, $-\nabla^2 + (1/c^2)(\partial^2/\partial t^2)$

Subscripts

b	=	value on blade surface
k	=	value for kth sinusoid
n	=	resolved in the surface normal direction
r	=	resolved in the radiation direction
0	=	value in stationary undisturbed flow
∞	=	value at infinite distance

Superscripts

-	=	time-averaged component/generalized variable
$'$	=	time-fluctuating component

Introduction

At present helicopter cruise speeds, the flow near the tip of the blade becomes transonic during the advancing phase of the cycle, which is when most of the noise is produced. Shock-associated rotor noise is consequently an important noise source, but predicting it in a way which is sufficiently fast and physically insightful to be useful to rotor designers remains a major challenge.

A good basis for predicting transonic rotor noise is provided by the permeable surface form of the Ffowcs Williams–Hawkings[1] (FW–H) equation (see Refs. 2–4). This expresses the noise in terms of a distribution of monopole and dipole sources over a permeable control surface and a distribution of quadrupole sources over the

Received 15 December 2003; accepted for publication 27 May 2004.

*Ph.D. Student, Department of Engineering. Student Member AIAA.
†Professor, Mechanical Engineering, and Head, Division of Energy, Fluid Mechanics and Turbomachinery. Senior Member AIAA.

volume outside of the surface. The noise from the volume distribution is numerically impractical to compute, but is negligible if the volume contains only subsonic flow.[5–7] This is consistent with the observation that the noise from the entire flow volume is negligible up to blade Mach numbers of approximately 0.8 (Refs. 8 and 9).

By choosing a permeable control surface that encloses the blade and all transonic flow regions, it can therefore be ensured that the volume term in the FW–H equation is negligible, leaving only the more straightforward surface terms. Also, when the control surface is chosen to be close to the blade, the computational effort required to calculate the control surface flow variables is minimized.

With the volume term neglected, the permeable surface form of the FW–H equation represents the sound as being generated by acoustic sources on the control surface. Whereas these acoustic sources do not represent the physical sources of sound, they do generate an equivalent sound field. For straightforward helicopter motion including hover and steady forward flight, it is possible to calculate the acoustic sources directly using unsteady computational fluid dynamics (CFD) solvers. However, for more complicated motion, particularly for maneuvering helicopters, computation of the acoustic sources using CFD solvers becomes too time consuming to generate noise predictions in timescales that are useful to blade designers.

To obtain the acoustic sources more efficiently, low-order modeling may be used. Given information on the unsteady variation of the flight conditions and computed values of the acoustic sources under certain flight conditions, low-order models enable the resulting temporal variation of the acoustic sources to be approximated. Models for the dynamics of the thickness and loading noise of subsonic rotor blades have been successfully developed,[10–12] and it is now proposed that suitable models for the acoustic sources at transonic speeds are obtained.

A variety of techniques are available for developing low-order models. Those commonly used when the dynamics are nonlinear include representing the system in terms of its eigenmodes and eigenvalues[13,14] and using the Volterra theory of nonlinear systems.[15] If the system dynamics are essentially linear then it is often more efficient to make use of linear techniques such as indicial methods[10–12,16] and system identification.[17,18]

For transonic flows, such as those around a helicopter blade, the steady-state flowfield is inherently a nonlinear function of flight condition. However, for sufficiently small variations in flight condition, the dynamics of the unsteady flowfield are likely to be linear about this steady state. That is, it may be possible to consider the unsteady flowfield as a linear perturbation about the quasi-steady field.[13,19] The system is said to be dynamically linear, and the unsteady fluctuations may be modeled using techniques appropriate for linear systems.

In this work, low-order models are developed using system identification. This is a technique for developing mathematical models of dynamically linear systems based on observed system data.[17,18] The parameters of a model structure are fitted to measured input and output system data. The accuracy of the model then depends on the choice of the model structure and the quantity and quality of data used. The technique has recently been used with success in approximating unsteady CFD solutions around complex bodies[20] and in approximating flame transfer functions in combustion oscillations.[21]

Although the acoustic sources provide sufficient information for noise prediction, because they are on a permeable control surface and are therefore fictitious sources, it is difficult to attach physical meaning to their dynamics. It is known that at transonic speeds, noise originating at the shock surfaces is a significant component of the overall noise.[6,22] By also studying the dynamic behavior of the shock and relating this to the dynamics of the acoustic sources, it is likely that some physical insight into the unsteadiness of the acoustic sources can be extracted.

The shock wave is straightforward to define in terms of its position and strength, and its properties are unaffected by the choice of control surface. These factors, combined with the availability of some previous work on shock dynamics for comparison purposes,[23–26] suggest that obtaining low-order models for the shock wave will be a more straightforward task than for the acoustic sources. Hence, modeling the dynamic behavior of the shock provides a good base from which to progress to the dynamics of the acoustic sources.

Although the benefits of low-order modeling will be most tangible for three-dimensional flows, it is less complicated and time consuming to build up an understanding of low-order modeling techniques and an insight into the acoustic source behavior through two-dimensional flow. The following work was carried out using a two-dimensional Euler CFD solver incorporating high-resolution shock-capturing techniques (developed by S. A. Karabasov and T. P. Hynes, Cambridge University Engineering Department, United Kingdom[27]) in which both the blade speed and blade pitch angle could be varied.

The response of the shock wave to flight condition variations is first considered, followed by the responses of the integrals of the acoustic sources over the control surface contour.

Shock Dynamics: Preliminary Modeling

Because noise originating at the shock surfaces is a significant component of helicopter noise at transonic speeds,[6,22] the dynamics of the shock wave were first considered. The two-dimensional Euler solver was used to simulate the transonic flow over a NACA0012 airfoil of chord 0.5 m. It was ensured that a shock wave existed only on the upper blade surface, and its response to variations in blade speed and blade pitch angle was recorded.

To consider the effect of varying the blade speed, the blade pitch angle was kept constant at 3.66 deg and the blade speed was varied sinusoidally as $v(t) = \bar{v} + \hat{v}\cos(\omega t)$. Similarly, to consider the effect of a varying blade pitch angle, the blade speed was fixed at 262.2 ms^{-1} and the blade pitch angle was varied sinusoidally as $\alpha(t) = \bar{\alpha} + \hat{\alpha}\cos(\omega t)$.

The effect of varying the frequency of oscillation at fixed amplitude was considered, followed by the effect of varying the oscillation amplitude at fixed frequency. With the exception of one case, the shock remained well formed throughout the oscillation and did not approach the emergence/disappearance regime. The fixed frequency was chosen to be 170 rads^{-1}, the associated period being approximately equal to the time for which the blade speed would lie within the given range under typical rotation conditions.

The response of the shock position was recorded after two oscillations so that the essential features of the steady state rather than transient response were captured. The results for the blade speed variations and blade pitch angle variations are shown in Figs. 1 and 2, respectively. Figures 1a and 2a are for varying frequency with Figs. 1b and 2b for varying oscillation amplitudes.

In Figs. 1 and 2, the shock position is seen to undergo limit-cycle oscillations. The amplitude of these increases with the amplitude of the input oscillations and decreases with oscillation frequency. Hysteresis is evident; the shock position for a given blade speed/pitch angle is not the quasi-steady value, but depends on whether the speed/pitch angle is increasing or decreasing. The curves are followed in an anticlockwise direction, so that for a given speed/pitch angle the shock is further back when the speed/pitch angle is decreasing and farther forward when it is increasing. This corresponds to type A shock motion as classified by Tijdeman and Seebass.[23]

The tilted ellipse shapes in Figs. 1 and 2 suggest that the shock position may depend on a time-delayed value of the blade speed. That is, there may be a phase shift between the blade speed and the shock position, behavior that is consistent with that described by Tijdeman and Seebass.[23] Figure 3 shows graphs of $\cos(t - T_d)$ against $\cos(t)$, where T_d is a time delay, and demonstrates the effect of time delays. There is a clear likeness to the curves in Figs. 1 and 2.

To investigate the possibility of simple time delay models, the coefficients A and B and the time delay T_d that gave best fit to the following relationship, where f is either the blade speed or blade pitch angle, were calculated for each of the cases in Figs. 1 and 2. Figs. 4 and 5 show graphs of i_s against $f(t - T_d)$ for the best fit value of T_d; the accuracy of the time-delay model can be assessed by the extent to which both sides of the hysteresis curve collapse

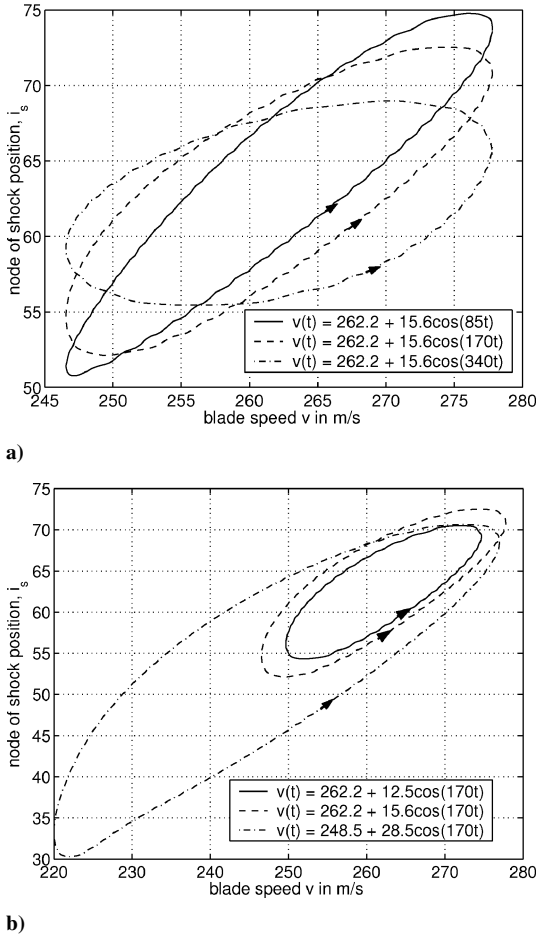

Fig. 1 Shock position due to a sinusoidally varying blade speed.

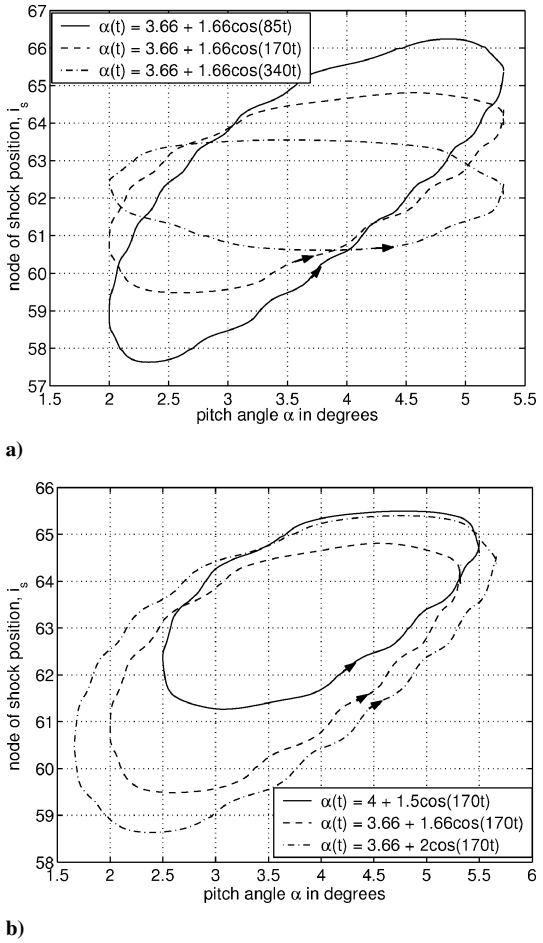

Fig. 2 Shock position due to a sinusoidally varying blade pitch angle.

onto one another to form a single line,

$$\begin{aligned} i_s(t) &= A + Bf(t - T_d) \\ &= A + B\bar{f} + B\hat{f}\cos[\omega(t - T_d)] \\ &= A + B\bar{f} + B\hat{f}\cos(\omega t)\cos(\omega T_d) + B\hat{f}\sin(\omega t)\sin(\omega T_d) \end{aligned} \tag{1}$$

For all of the cases in which the shock wave remains well formed throughout the oscillation, the two sides of each curve have collapsed well onto one another, particularly at the higher two frequencies. For the case in which the shock approaches the emergence/disappearance regime (the large-amplitude case, Fig. 4a), the two sides of the curve collapse almost exactly onto one another while the shock is well formed, but the collapse is less good when the emergence/disappearance regime is approached. The values of the time delay that give best collapse vary with frequency. Where the start/end points of the curves do not quite join up, this is due to small levels of transients contaminating the steady-state response.

These results suggest that a simple time delay provides a good model of the response of the shock position to blade speed and blade pitch angle variations when the shock is well developed, but is less accurate when the shock approaches the emergence/disappearance regime. The value of the time delay is frequency dependent.

Frequency-dependent time delays indicate the possibility of first-order lag relationships. Such relationships are characterized by the following differential equation, where $f'(t)$ is either the blade speed fluctuation or the blade pitch angle fluctuation, $i_s'(t)$ is the shock position fluctuation, T_c is a time constant, and E is an amplitude constant,

$$T_c\frac{\mathrm{d}i_s'}{\mathrm{d}t} + i_s'(t) = Ef'(t) \tag{2}$$

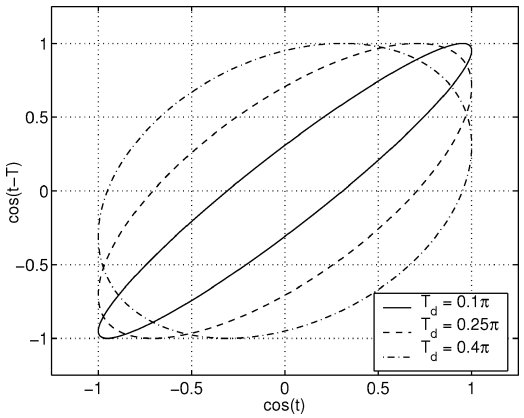

Fig. 3 Tilted ellipse shapes that arise from time delays, cos $(t - T_d)$ vs cos (t).

Taking Laplace transforms of Eq. (2), defining $f(s)$ and $i_s(s)$ to be the Laplace transforms of $f'(t)$ and $i_s'(t)$, respectively, and setting $s = i\omega$ gives the transfer function corresponding to a first-order lag relationship,

$$i_s(\omega)/f(\omega) = E/(i\omega T_c + 1) \tag{3}$$

For the input having a sinusoidal form, as in the cases being considered, the first-order lag results in a shock position response of the form,

$$i_s(t) = \frac{\left(E\hat{f}\big/T_c^2\right)\cos(\omega t)}{\left(1\big/T_c^2\right) + \omega^2} + \frac{\left(E\omega\hat{f}\big/T_c\right)\sin(\omega t)}{\left(1\big/T_c^2\right) + \omega^2} + \text{mean level} + \text{transients} \tag{4}$$

Table 1 First-order lag time constants corresponding to the time delays of best fit

$\bar{v}$, $\hat{v}$, ms^{-1}	ω, rads^{-1}	T_d, s	T_{cv}, s	$\bar{\alpha}$, $\hat{\alpha}$, deg	ω, rads^{-1}	T_d, s	$T_{c\alpha}$, s
262.2, 12.5	170	0.0037	0.0043	4, 1.5	170	0.0055	0.0080
262.2, 15.6	170	0.0038	0.0044	3.66, 1.66	170	0.0053	0.0074
262.2, 15.6	85	0.0045	0.0047	3.66, 2	170	0.0053	0.0075
262.2, 15.6	340	0.0032	0.0055	3.66, 1.66	85	0.0082	0.0099
				3.66, 1.66	340	0.0048	0.0090

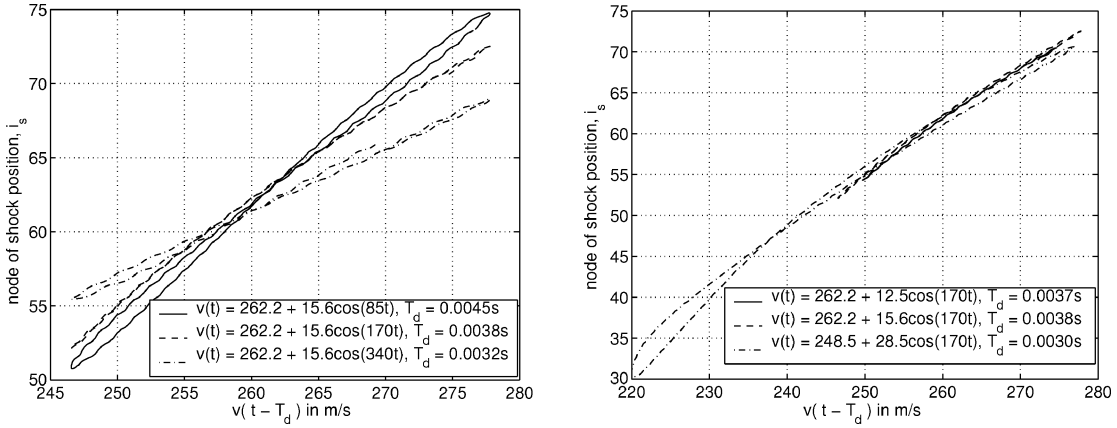

Fig. 4 Shock position vs time delayed blade speed for the time delays of best fit.

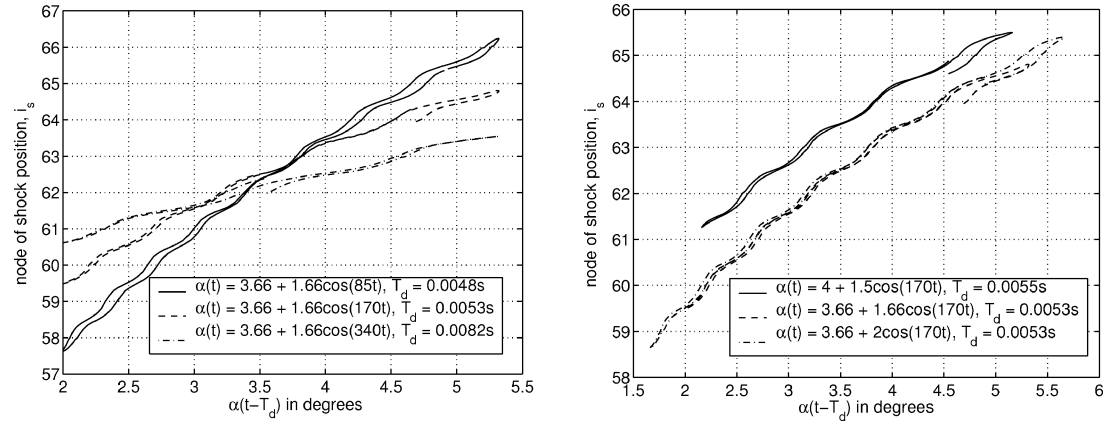

Fig. 5 Shock position vs time delayed blade pitch angle for the time delays of best fit.

Comparing the fluctuating terms in Eqs. (1) and (4) allows the time constant to be related to the oscillation frequency and measured time delay through $T_c = \tan(\omega T_d)/\omega$. The values of the time constants corresponding to the time delays of best fit are given in Table 1. Only those cases for which the shock is well developed throughout are included.

From Table 1, it can be seen that for the blade speed variations, the time constant varies little, particularly for the lower frequencies. For the blade pitch angle variations, the time constant is fairly consistent across the cases and is approximately twice as large as for the blade speed cases. This suggests that the variations of shock position with blade speed and blade pitch angle are well modeled by first-order lag relationships.

Shock Dynamics: System Identification

A more methodical approach is now used to obtain low-order models that are known to be accurate over the frequency range of interest. Assuming (and later confirming) that the unsteady variations are sufficiently small for the flowfield to be dynamically linear, a system identification approach can be used.

The input in the system to be modeled is either the blade speed fluctuation $v'(t)$, or the pitch angle fluctuation $\alpha'(t)$, and the output is the shock position fluctuation $i_s'(t)$. It is the fluctuations that are of interest as the mean levels are related through the nonlinear quasi-steady relationship that can be obtained separately from a steady CFD solver. Input and output data are obtained by sampling the relevant variables in the CFD simulations at discrete times. The aim of the system identification is then to model the relationship between the relevant input fluctuations and the shock position fluctuations by approximating the form of the transfer functions,

$$H_1(\omega) = i_s(\omega)/v(\omega), \qquad H_2(\omega) = i_s(\omega)/\alpha(\omega) \tag{5}$$

Form of the Input Signal

An important issue in system identification is the form of the input signal. The input in these cases is either the blade speed fluctuation or the blade pitch angle fluctuation specified in the CFD solver, and care must be taken to ensure that their signals have numerically practical forms. The choice of input signal is an issue that has been addressed in some detail by Ljung[17] and Zhu et al.[21] The main options with their merits and drawbacks are outlined next.

One approach is to force the system harmonically at particular frequencies, as carried out in the preliminary modeling. For a variety of frequencies, the shock position response due to a harmonically varying input can be measured. Once the initial transients have died away, the magnitude and phase of the transfer function at the forcing frequency can be deduced. The problem with this approach is

that each calculation yields information at just one frequency, and many calculations are therefore needed. Computations are very time consuming as they must be continued until all transients have died away.

A better approach is to choose an input signal that contains a range of frequencies, so that broadband information can be deduced from a single calculation. In theory, a Dirac delta or impulse function contains all frequencies, although it is numerically impossible to implement in a CFD code. It is, however, possible to implement a short-duration pulse; the pulse will not contain all frequencies, but will contain the frequencies of interest if the duration is sufficiently short. Because of the short duration, it is preferable to process data in the time domain before progressing to the frequency domain. The linear relationship between the output signal $i'_s(t)$ and the input signal $f'(t)$ can be expressed in the form of an infinite impulse response (IIR) filter.[17,18] The filter describes the output as a linear combination of previous outputs and present and previous inputs and is very easy to implement recursively. For a sampling period T, it has the form

$$i'_s(t) = \sum_{i=0}^{I} a_i f'(t - iT) + \sum_{j=1}^{J} b_j i'_s(t - jT) \tag{6}$$

The filter order is (I, J), and the filter coefficients are a_i and b_j. The coefficients are found by fitting the right-hand side of Eq. (6) to $i'_s(t)$. Once the IIR filter coefficients are known, the transfer function $H(\omega)$ can be found by taking z transforms and substituting in $z = e^{i\omega T}$. If the z transforms of $i'_s(t)$ and $f'(t)$ are $i_s(z)$ and $f(z)$, respectively, this gives

$$H(\omega) = \frac{i_s(z)}{f(z)} = \frac{\sum_{i=0}^{I} a_i z^{-i}}{1 - \sum_{j=1}^{J} b_j z^{-j}} \tag{7}$$

Although this input signal results in a rapid CFD calculation (due to the short time pulse) and provides broadband information from a single calculation, it does have one drawback. The error caused by the noise in the system is inversely proportional to the amplitude of the pulse,[17] but the pulse must be low enough in amplitude to result in a linear response. These conflicting requirements often result in a linear response being associated with significant noise error.

To utilize an input signal that contains a range of frequencies but that does not suffer from noise/linearity tradeoff limitations, a sum of sines approach can be used. This involves an input signal that comprises many sinusoids at different frequencies,

$$f'(t) = \hat{f} \sum_{k=1}^{K} \sin(\omega_k t + 2\pi\phi_k) \tag{8}$$

The lower and upper limits of the passband are $\omega_{\min}$ and $\omega_{\max}$, K is the number of sinusoids spread equally over the passband, and $\omega_k = \omega_{\min} + (k-1)(\omega_{\max} - \omega_{\min})/(K-1), k = 1 \ldots K$. To ensure a sensible time variation of the signal amplitude, the phase of the kth sinusoid at $t = 0$ is $2\pi\phi_k$, where ϕ_k is a random number chosen from a uniform distribution on the interval (0, 1). Here, $\hat{f}$ is simply a scaling constant. Fitting is again performed in the time domain using the IIR filter model structure given in Eq. (6).

Methodology

Based on the preceding discussion, input signals based on the sum of sines approach were used. Because harmonic forcing at three different frequencies had already been carried out at a mean blade speed of 262.2 ms^{-1} and a mean pitch angle of 3.66 deg, system identification was performed at these mean levels.

For the blade speed input system identification, the blade pitch angle was set to 3.66 deg, and the blade speed had the form

$$v(t) = \bar{v} + \hat{v} \sum_{k=1}^{K} \sin(\omega_k t + 2\pi\phi_k) \tag{9}$$

where $\bar{v} = 262.2\ \text{ms}^{-1}$, whereas for the blade pitch angle input system identification, the blade speed was set to 262.2 ms^{-1} and the blade pitch angle had the form

$$\alpha(t) = \bar{\alpha} + \hat{\alpha} \sum_{k=1}^{K} \sin(\omega_k t + 2\pi\phi_k) \tag{10}$$

where $\bar{\alpha} = 3.66$ deg.

For both simulations, the lower passband limit was chosen to be $\omega_{\min} = 6\ \text{rads}^{-1}$, corresponding to a reduced frequency based on the half-chord and mean blade speed of 0.0057. Assuming a slightly larger time delay than the maximum observed in the harmonic testing, the phase lag at this frequency should be negligible. (A time delay of T_d seconds corresponds to a frequency domain response $e^{-i\omega T_d}$.) The upper passband limit $\omega_{\max}$ was chosen to be much larger than the typical rotational frequency of a helicopter blade to give $\omega_{\max} = 680\ \text{rads}^{-1}$, corresponding to a reduced frequency of 0.65.

The number of sinusoids K was chosen to be 338, which resulted in the input signal containing frequencies at intervals of 2 rads^{-1}. To ensure that the input/output data contained sufficient information on all component frequencies and to maximize the efficiency of the system identification process,[17] a whole number of input signal periods was considered. Because all component frequencies were multiples of 2 rads^{-1}, this meant that the data from the CFD simulation was required over a multiple of π seconds.

The normalization speed $\hat{v}$ and pitch angle $\hat{\alpha}$ were chosen to ensure that the shock did not become unrealistically strong and that it did not approach the emergence/disappearance regime. The former constraint was more limiting, and so $\hat{v} = 0.6$ and $\hat{\alpha} = 0.08$ were chosen, resulting in a maximum blade Mach number of approximately 0.8 for the blade speed variation and a maximum blade pitch angle of approximately 7 deg for the blade pitch angle variation.

In the CFD simulations, the chosen input was increased smoothly from zero to the mean level before adding the sum of sines component, ensuring throughout that both the input and its first time derivative were continuous. Input and output data were only analyzed well after the mean speed was reached, to reduce the contamination due to transients from the initial increase. The input time variations for the two different CFD simulations are shown in Fig. 6.

The model structure used in the system identification was that of an IIR filter with a model for the error $e(t)$ incorporated. The error model allowed the error behavior to vary with frequency. This is known as an autoregressive moving average extra (ARMAX) model,[17,18,28] and its structure for a sampling period T, input signal $f(t)$, and output signal $i_s(t)$ is

$$i'_s(t) = \sum_{i=0}^{I} a_i f'(t - iT) + \sum_{j=1}^{J} b_j i'_s(t - jT) + \sum_{l=0}^{L} d_l e(t - lT) \tag{11}$$

The autoregressive part consists of the earlier outputs,

$$\sum_{j=1}^{J} b_j i'_s(t - jT)$$

the moving average part is

$$\sum_{l=0}^{L} d_l e(t - lT)$$

and the extra input is

$$\sum_{i=0}^{I} a_i f'(t - iT)$$

The filter order is strictly given by (I, J, L), although (I, J) is sufficient to describe the resulting transfer function from input to output. The system identification procedure aims to find the values of the coefficients, a_i, b_j, and d_l, which give best fit to the CFD data for a given filter order.

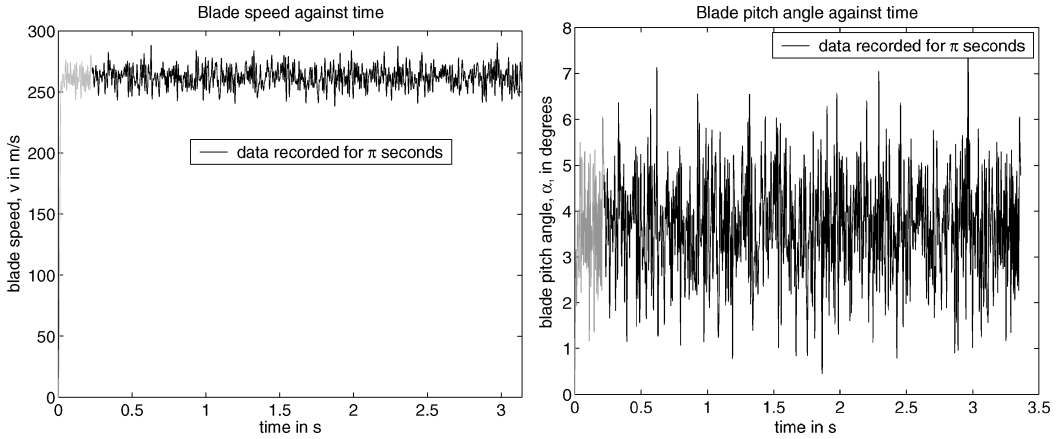

Fig. 6 Time variation of the input for the two different CFD simulations.

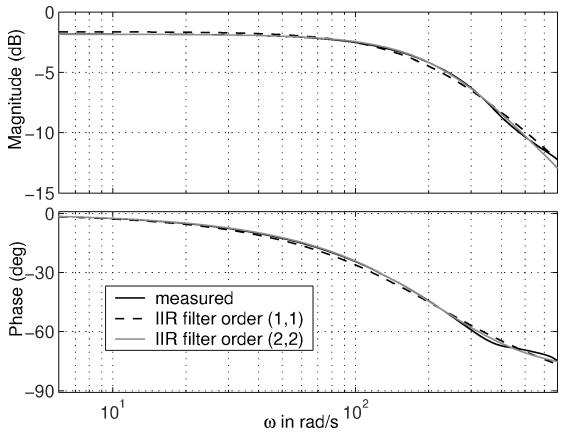

Fig. 7 Transfer function from blade speed fluctuation to shock position fluctuation.

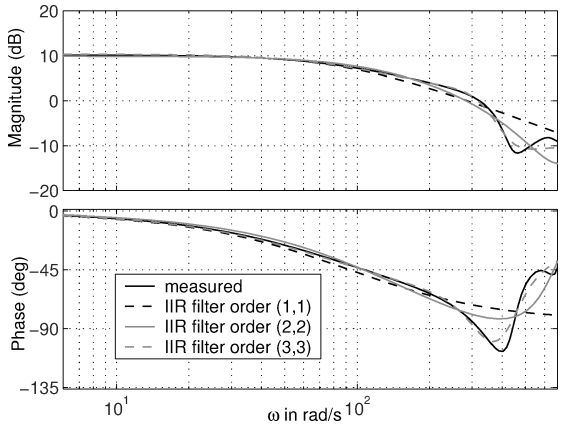

Fig. 8 Transfer function from blade pitch angle fluctuation to shock position fluctuation.

Results

The transfer functions from the blade speed and blade pitch angle variations to the shock position variation are shown in Figs. 7 and 8, respectively. In both of these figures, the measured frequency response (obtained by fitting a very high-order filter to the measured data so that convergence with filter order had been obtained) is compared to the frequency responses predicted by low-order IIR filters.

The magnitude of both measured frequency responses is flat at low frequencies, falls off at higher frequencies, and exhibits no resonances. The phase of both responses decreases gradually from zero to approximately −90 deg. This behavior indicates approximate first-order lag relationships.

An IIR filter of order (1, 1) describes the frequency response for the blade speed input extremely accurately and the frequency response for the blade pitch angle input reasonably accurately. In both cases, the fit deteriorates as frequency increases. The form of these filters (neglecting the error term) for a sampling period of $T = 9.04 \times 10^{-5}$ s is

$$i_s'(t) = -0.00939v'(t) + 0.0249v'(t-T) + 0.981i_s'(t-T) \quad (12)$$

$$i_s'(t) = 0.0323\alpha'(t) - 0.00513\alpha'(t-T) + 0.9921i_s'(t-T) \quad (13)$$

Filters of order (1, 1) require output data at just one initial time level to predict the response to an input. The good fit offered by the filters of order (1, 1) therefore suggests that the dynamics of the system are straightforward. Approximating the equivalent continuous time transfer functions by applying the Tustin transform and simplifying for the given frequency range gives

$$H_1(\omega) = \frac{i_s(\omega)}{v(\omega)} = \frac{173}{i\omega + 209} = \frac{0.828}{0.00479i\omega + 1} \quad (14)$$

$$H_2(\omega) = \frac{i_s(\omega)}{\alpha(\omega)} = \frac{302}{i\omega + 92} = \frac{3.27}{0.0108i\omega + 1} \quad (15)$$

These correspond exactly to first-order lag relationships and generalize the phase lag findings of Tijdeman and Seebass.[23] The time constants are 0.00479 s for the blade speed input and 0.0108 s for the blade pitch angle input. These compare favorably with the average time constants of 0.0047 and 0.0084 s obtained from harmonic forcing in the preliminary modeling. The better agreement of the blade speed input time constants would be expected because the IIR filter frequency response gave a better fit to the measured transfer function.

Test of Linearity

To demonstrate that the shock position response at a mean blade speed of 262.2 ms^{-1} and a mean pitch angle of 3.66 deg was dynamically linear, the effect of changing the size of the blade speed fluctuations was considered. For a dynamically linear response, this should not alter the form of the transfer function between the blade speed fluctuation and the shock position fluctuation.

The blade pitch angle was held constant and a sum of sines blade speed with a mean level of 262.2 ms^{-1} and fluctuating amplitude of $\hat{v} = 0.8\ \text{ms}^{-1}$ was applied. The fluctuating amplitude was larger than that used earlier, but the shock still remained well formed throughout the simulation. The time variation of the blade speed is compared to that used earlier in Fig. 9. The same system identification techniques were applied, and the transfer function in Fig. 10 was obtained.

The transfer function is almost identical to that obtained using the smaller blade speed fluctuations (Fig. 7). The continuous time form of the order (1, 1) IIR filter is $174/(i\omega + 211)$, which is in very close agreement to that obtained earlier.

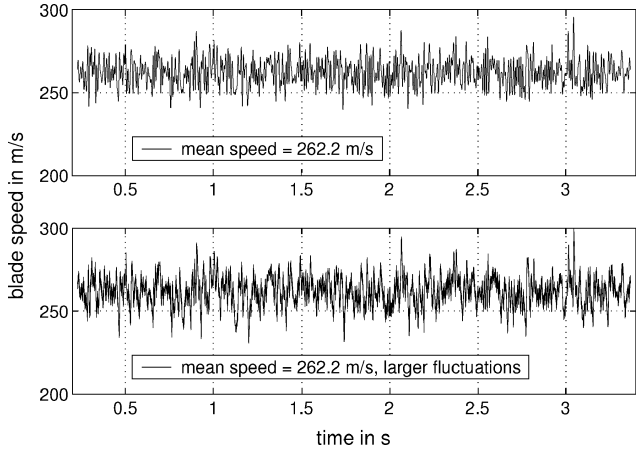

Fig. 9 Comparison of the blade speed variation with that of the preceding case (top).

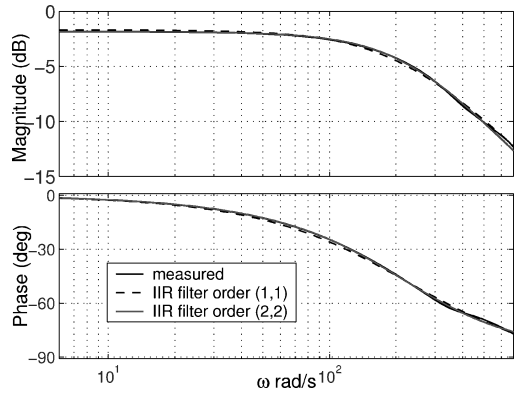

Fig. 10 Transfer function from blade speed fluctuation to shock position fluctuation for larger blade speed fluctuations.

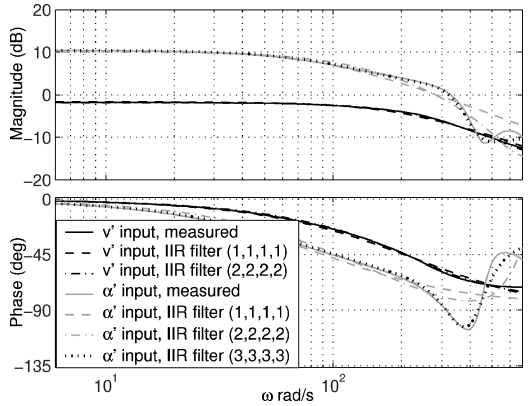

Fig. 11 Two frequency responses for the dual-input CFD simulation.

This confirms that the response of the shock position is dynamically linear at the mean conditions being considered. If the amplitude of the blade speed fluctuations was significantly increased, or if a lower mean blade speed/blade pitch angle was considered so that the emergence/disappearance regime of the shock was approached, the shock position response would no longer be expected to be dynamically linear. However, the main noise generating regime is likely to involve large shock strengths and a well-formed shock, meaning that the more complex dynamics expected at shock emergence/disappearance are unlikely to be as relevant to noise prediction.

System Identification for Two Inputs

In the two-dimensional CFD code, the blade speed and blade pitch angles can be varied simultaneously. The possibility of obtaining the transfer functions from blade speed and blade pitch angle to shock position in a single calculation is now considered. For a linear system, the output resulting from more than one input is equal to the sum of the outputs seen when each of the inputs is applied individually. This means that if the shock position response is dynamically linear, the transfer functions predicted when the two inputs vary simultaneously should be the same as those obtained for the separate single-input cases.

The CFD system in which both the blade speed and blade pitch angles vary simultaneously is a dual-input system. Both input signals can be formed using the sum of sines approach as in the single-input case, but to ensure that the inputs are independent the frequencies contained in each signal should be different while extending over the same passband.[17] The input signals for the simultaneous blade speed and blade pitch angle inputs were

$$v(t) = \bar{v} + \hat{v} \sum_{k_1=1}^{K_1} \sin\left(\omega_{k_1} t + 2\pi\phi_{k_1}\right) \tag{16a}$$

$$\alpha(t) = \bar{\alpha} + \hat{\alpha} \sum_{k_2=1}^{K_2} \sin\left(\omega_{k_2} t + 2\pi\phi_{k_2}\right) \tag{16b}$$

where $\bar{v} = 262.2\ \text{ms}^{-1}$, $\hat{v} = 0.6\ \text{ms}^{-1}$, $\bar{\alpha} = 3.66$ deg, $\hat{\alpha} = 0.08$ deg, $\omega_{k_1} = 4 + 4(k_1 - 1)$, $\omega_{k_2} = 6 + 4(k_2 - 1)$, $K_1 = K_2 = 170$, and ϕ_{k_1} and ϕ_{k_2} are again random phases chosen from the range (0, 1). The frequencies contained in the blade speed and blade pitch angle inputs therefore interleave one another over the same passband.

The system identification model structure was again based on that of an IIR filter. Because of the presence of two inputs, its form is most easily expressed in terms of the z transform of the IIR filter. If $v(z)$, $\alpha(z)$, and $e(z)$ are the z transforms of $v'(t)$, $\alpha'(t)$, and $e(t)$, respectively, this gives

$$i_s(z) = \frac{\sum_{i_1=0}^{I_1} a_{i_1} z^{-i_1}}{1 - \sum_{j_1=1}^{J_1} b_{j_1} z^{-j_1}} v(z) + \frac{\sum_{i_2=0}^{I_2} a_{i_2} z^{-i_2}}{1 - \sum_{j_2=1}^{J_2} b_{j_2} z^{-j_2}} \alpha(z) + \frac{\sum_{k=0}^{K} c_k z^{-k}}{1 - \sum_{l=1}^{L} d_l z^{-l}} e(z) \tag{17}$$

The order of this filter is strictly $(I_1, I_2, K, J_1, J_2, L)$, although the order (I_1, I_2, J_1, J_2) is sufficient to describe the transfer functions from inputs to output.

The frequency responses obtained are shown in Fig. 11. It can be seen that the predicted frequency responses are the same shape as those predicted in the single-input cases. The order (1, 1, 1, 1) filter is seen to give a good approximation to the measured responses, particularly at the lower frequencies. The continuous time transfer functions that this filter corresponds to over the frequency range of interest are

$$H_1(\omega) = \frac{i_s(\omega)}{v(\omega)} = \frac{177}{i\omega + 215} = \frac{0.826}{0.00466 i\omega + 1} \tag{18}$$

$$H_2(\omega) = \frac{i_s(\omega)}{\alpha(\omega)} = \frac{298}{i\omega + 90} = \frac{3.32}{0.0111 i\omega + 1} \tag{19}$$

These are in close agreement with the transfer functions obtained from the single-input calculations in Eqs. (14) and (15). This further confirms that the response of the shock position is dynamically linear.

Low-Order Models for the Acoustic Source Integrals

Having obtained an understanding of the two-dimensional dynamics of the shock wave, the same CFD/system identification approach was now applied to the control surface acoustic sources.

The acoustic sources can be defined through the differential form of the FW–H equation with the quadrupole term neglected. In this

form, the source descriptions do not depend on observer location,

$$\Box^2 p'(x,t) = -\frac{\partial}{\partial x_i}(L_i \delta(f)|\nabla_x f|) + \frac{\partial}{\partial t}(\rho_0 U_n \delta(f)|\nabla_x f|) \quad (20)$$

where $L_i = p_{ij} n_j + \rho u_i (u_n - v_n)$ and $U_n = (1 - \rho/\rho_0) v_n + \rho/\rho_0 u_n$.

The acoustic sources are the vector L_i and the vector component $\rho_0 U_n$, both considered at points that lie on the control surface.

From the following integral form of the FW–H equation, it is clear that if the time variations of L_i and $\rho_0 U_n$ at each point on the control surface can be predicted using low-order models, it will be possible to calculate the observer sound without requiring full CFD input data,

$$p'(\boldsymbol{x},t) = -\frac{\partial}{\partial x_i}\int_S \left[\frac{L_i A}{4\pi r|1-M_r|}\right]_{\tau *} \mathrm{d}S(\eta) + \frac{\partial}{\partial t}\int_S \left[\frac{\rho_0 U_n A}{4\pi r|1-M_r|}\right]_{\tau *} \mathrm{d}S(\eta) \quad (21)$$

In general, sound prediction will require low-order models for the acoustic sources at all control surface grid points in three-dimensional space. To demonstrate the principles of low-order modeling and obtain an insight into the dynamics of the acoustic sources while avoiding this quantity of information, two-dimensional flow has again been considered. The section of the control surface can then be taken as constant, and only the variation of acoustic sources along the contour of the section need be considered. In two-dimensional problems, the acoustic sources of interest are $\rho_0 U_n$, L_x and L_y.

If the section of the control surface is acoustically compact, retarded time variations across it are small and the acoustic sources combine in Eq. (21) as straightforward contour integrals multiplied by their associated length. Thus, under the conditions of two-dimensional flow and a compact surface section, low-order models to describe the dynamics of the following integrals,

$$\int_S \rho_0 U_n \,\mathrm{d}S, \qquad \int_S L_x \,\mathrm{d}S, \qquad \int_S L_y \,\mathrm{d}S \quad (22)$$

where S is a unit length of control surface, provide sufficient information for noise prediction. The surface section will be compact if the M_r term is sufficiently small and therefore depends on the observer location as well as the section motion.

Methodology

The responses of the acoustic source integrals to variations in both blade speed and blade pitch angle were considered. System identification was first carried out with each of these inputs in turn held constant while the other varied with the same form as for the single-input shock response simulations, given in Eqs. (9) and (10).

The system outputs were the three acoustic source contour integrals, given in Eq. (22). The section of the integration control surface is shown in Fig. 12. The lower portion of the control surface follows the blade surface, whereas the upper portion comes away from the blade surface to enclose the largest extent of the shock and transonic flow region.

For each of the outputs, the sampled CFD data were used to fit the coefficients of the ARMAX model structure given by the following equation, where $I'(t)$ is the fluctuation of a source integral and $f'(t)$ is the fluctuation of an input,

$$I'(t) = \sum_{i=0}^{I} a_i f'(t-iT) + \sum_{j=1}^{J} b_j I'(t-jT) + \sum_{l=0}^{L} d_l e(t-lT) \quad (23)$$

System identification was also carried out for the blade speed and blade pitch angle varying simultaneously, as a check that the response of the acoustic source integrals was dynamically linear.

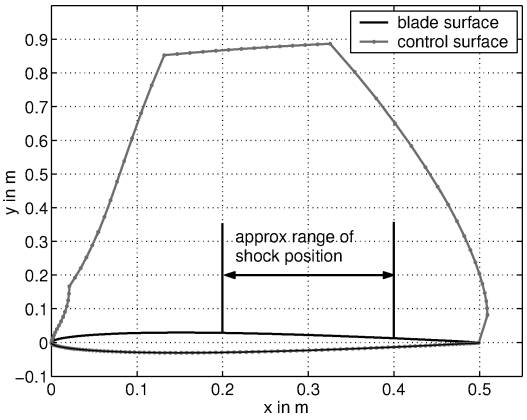

Fig. 12 Section of control surface.

The variations in the two input parameters had the same form as for the dual-input shock dynamics system identification, given in Eq. (16).

The sampled data were used to fit the coefficients of the following model filter structure, involving input and output fluctuations and expressed in terms of its z transform:

$$I(z) = \frac{\sum_{i_1=0}^{I_1} a_{i_1} z^{-i_1}}{1 - \sum_{j_1=1}^{J_1} b_{j_1} z^{-j_1}} v(z) + \frac{\sum_{i_2=0}^{I_2} a_{i_2} z^{-i_2}}{1 - \sum_{j_2=1}^{J_2} b_{j_2} z^{-j_2}} \alpha(z) + \frac{\sum_{k=0}^{K} c_k z^{-k}}{1 - \sum_{l=1}^{L} d_l z^{-l}} e(z) \quad (24)$$

Results

The measured and fitted frequency responses for the single-input simulations are shown for the three integrals in Fig. 13. The responses for $\int_S L_y \,\mathrm{d}S$ resemble those for shock position; fall offs in both gain and phase occur at similar frequencies, although the fall offs are more rapid than for the shock position. The responses of $\int_S L_x \,\mathrm{d}S$ and $\int_S \rho_0 U_n \,\mathrm{d}S$ both resemble high-pass rather than low-pass filters, and as such are quite different to the shock position responses. The shapes of the responses to the blade pitch angle input are similar to those for the blade speed input for all three integrals, although the magnitudes and the changeover frequencies differ.

Whereas an IIR filter of order (1, 1) described the shock position response to blade speed with sufficient accuracy, higher-order filters are required for the integrals of the acoustic sources. Increasing the filter order generally improves the accuracy of the prediction, but also increases the likelihood of unstable poles. For all three integrals, filters of order (2, 2) were felt to offer a good compromise.

The measured and fitted frequency responses for the dual-input simulation are shown for the three integrals in Fig. 14. Filters of order (2, 2, 2, 2) were found to describe the responses with reasonable accuracy; for clarity only this filter order is included for Fig. 14. The form of the frequency responses are seen to be the same as those for the single-input simulations in Fig. 13. This confirmed that the behavior of the acoustic sources was dynamically linear.

Noise Prediction

The filters in their discrete form are essentially difference equations and as such are straightforward to implement numerically. Complete information on how the blade speed varies allows the temporal variation of the acoustic source integrals to be predicted via a recursive calculation.

The integrals of the acoustic source integrals can be used for sound prediction if the flow is two dimensional and the surface section sufficiently compact. Such a case was considered, involving an infinitely long blade of constant cross section. The blade pitch angle was held constant at 3.66 deg and the blade speed varied sinusoidally as $v(t) = 262.2 + 15.6\cos(100t)$. The sound originating from the central 1-m length was considered at an observer whose

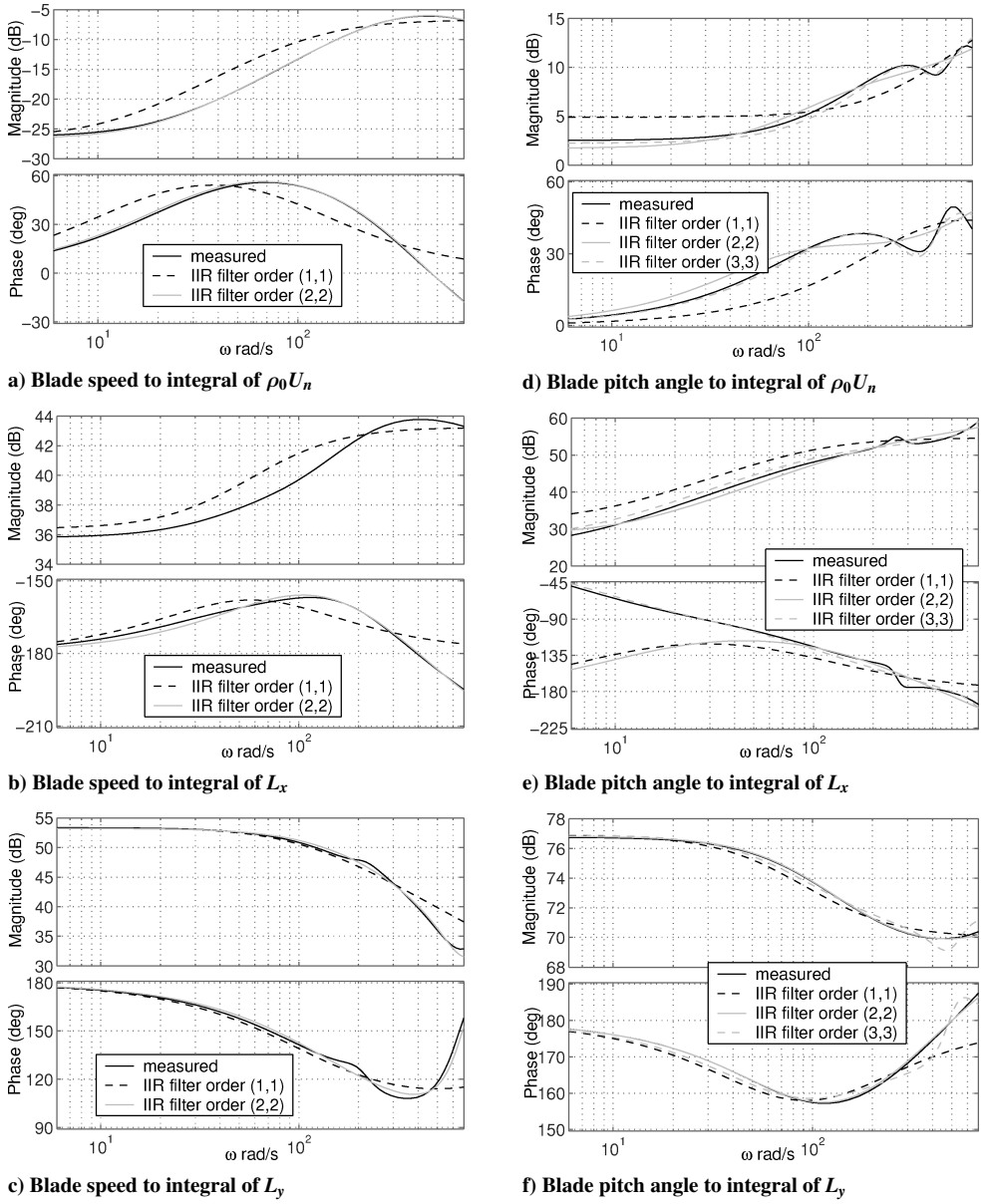

a) Blade speed to integral of $\rho_0 U_n$

b) Blade speed to integral of L_x

c) Blade speed to integral of L_y

d) Blade pitch angle to integral of $\rho_0 U_n$

e) Blade pitch angle to integral of L_x

f) Blade pitch angle to integral of L_y

Fig. 13 Transfer functions from blade speed and blade pitch angle to acoustic source integrals for single-input system identification.

position was fixed in the frame of the blade. The observer location was chosen so that the maximum value of M_r at any point on the permeable control surface was 0.6, which was sufficiently low to justify the assumption of compactness.

The time variation of the total sound at the observer location was then calculated using the permeable surface form of the FW–H equation in three different ways: 1) by calculating the retarded time at each point on the control surface and using full CFD data, 2) by assuming constant retarded time across the section of the control surface and using full CFD data, and 3) by assuming constant retarded time across the surface section and using low-order models for the acoustic source integrals instead of CFD data.

The agreement between the first two is a measure of the surface section compactness; the agreement between the latter two is a measure of how well the low-order models are performing. The results in Fig. 15 show that all three are in close agreement, confirming that low-order models are able to replace the need for a full CFD simulation in noise prediction. The variation of the acoustic source integrals throughout the cycle compared to that predicted by the low-order models is also shown. This level of accuracy is achieved with filters of order just $(2, 2)$; by increasing the filter orders, the accuracy could be improved still further.

The preceding section has demonstrated that low-order models can be used to replace the need for a full CFD simulation in two-dimensional noise predictions. The methodology would be much the same for three-dimensional flow, the main difference being that models for the acoustic sources $\rho_0 U_n$, L_x, L_y, and L_z would need to be derived for those points on the control surface that contributed significantly to the integrals.

Understanding the Low-Order Models

To gain an insight into how the dynamics of the acoustic source integrals are related to the dynamics of the shock position, the flow conservation equations were considered under the constraint that the blade pitch angle was fixed and only the blade speed could vary. These allowed the integrals of the acoustic sources to be related to the flow variables in the volume enclosed between the blade surface and the permeable control surface.

It was then assumed that the flow variables in the volume enclosed between the blade surface and permeable control surface were uniform either side of the shock, but underwent a step change across it. Because this is equivalent to assuming that the only unsteadiness of the flow variables within the enclosed volume is due to the motion of the shock, the agreement of the resulting predictions with the earlier obtained transfer functions provides a measure of the extent to which the dynamics of the acoustic source integrals are caused by the shock motion.

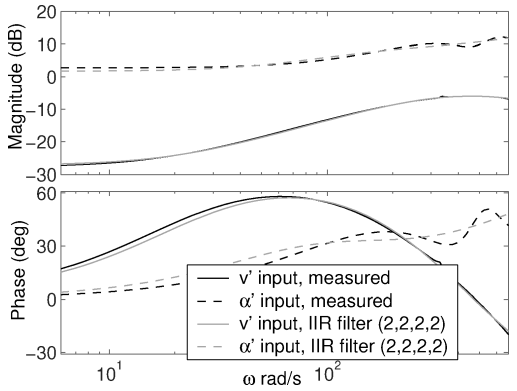

a) Integral of $\rho_0 U_n$

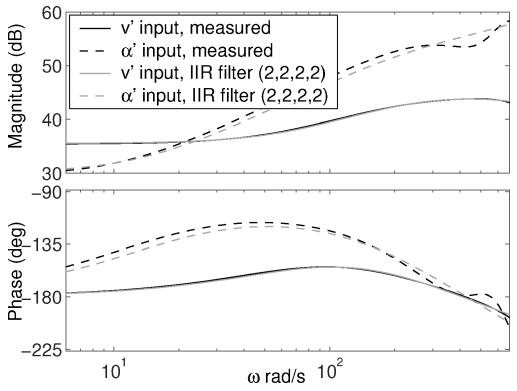

b) Integral of L_x

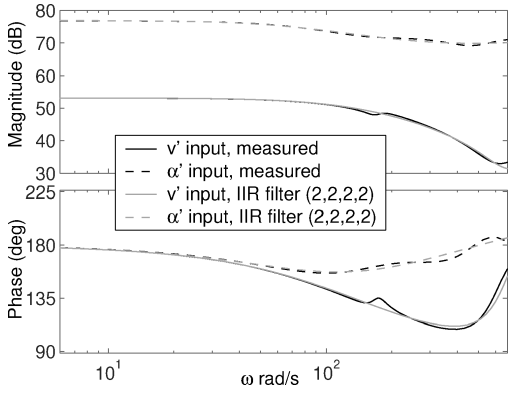

c) Integral of L_y

Fig. 14 Transfer functions from blade speed and blade pitch angle to acoustic source integrals for dual-input system identification.

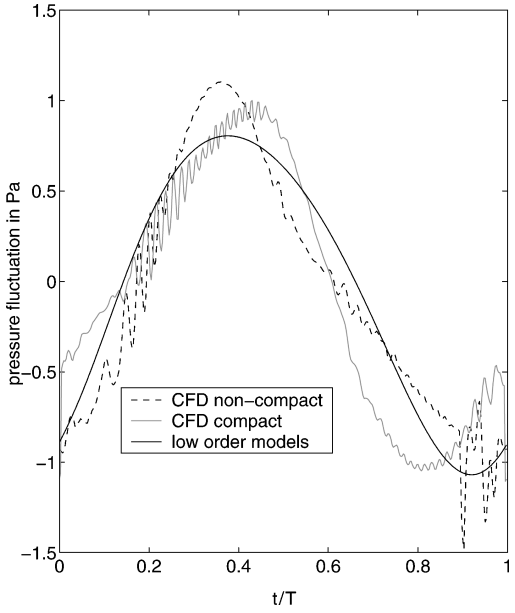

a) Variation of noise for one period of motion

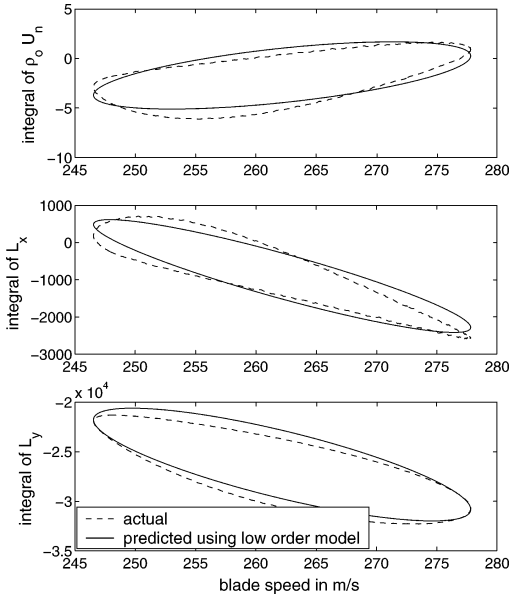

b) Variation of acoustic source integrals throughout the cycle

Fig. 15 Comparison of the observer sound and cyclic behavior of the acoustic source integrals as predicted by the CFD calculations and the low-order models.

The system considered is shown diagrammatically in Fig. 16. The permeable control surface over which the acoustic source integrals are considered is denoted by S_1, and the blade surface is denoted by S_2. The permeable control surface is coincident with the lower blade surface, but comes away from the upper blade surface to enclose closely the largest extent of the transonic flow region. The volume between the blade surface and control surface then contains a supersonic flow pocket, a shock wave, and a subsequent region of subsonic flow; the volumes of the supersonic and subsonic regions vary with shock position. Both surfaces move with velocity $\boldsymbol{v}$.

Denoting generalized variables by an overbar, and in the first instance defining them to have the values of the real flow variables outside of the permeable control surface S_1 and to be zero within it, the continuity equation valid over all space is

$$(\boldsymbol{\rho}_0 u_n + \rho'(u_n - v_n))\delta(f)|\nabla_x f| = \frac{\partial \overline{\rho'}}{\partial t} + \frac{\partial(\overline{\rho u_i})}{\partial x_i} \qquad (25)$$

Equation (25) is for a stationary reference frame. Because it is more physically intuitive to consider time derivatives in a frame that moves with the surfaces, the standard time derivatives are replaced by convective derivatives, $\mathrm{D}_v/\mathrm{D}t$,

$$\frac{\partial \overline{\rho'}}{\partial t} = \frac{\mathrm{D}_v \overline{\rho'}}{\mathrm{D}t} - v_i \frac{\partial \overline{\rho'}}{\partial x_i} \qquad (26)$$

Substituting in and then integrating over all space gives

$$\int_{S_1} (\boldsymbol{\rho}_0 u_n + \rho'(u_n - v_n))\,\mathrm{d}S = \int_{V_\infty} \frac{\mathrm{D}_v \overline{\rho'}}{\mathrm{D}t}\,\mathrm{d}V$$

$$- \int_{V_\infty} v_i \frac{\partial \overline{\rho'}}{\partial x_i}\,\mathrm{d}V + \int_{V_\infty} \frac{\partial(\overline{\rho u_i})}{\partial x_i}\,\mathrm{d}V \qquad (27)$$

If attention is restricted to cases in which the blade pitch angle is constant and only the blade speed varies, the surface velocity $\boldsymbol{v}$ is

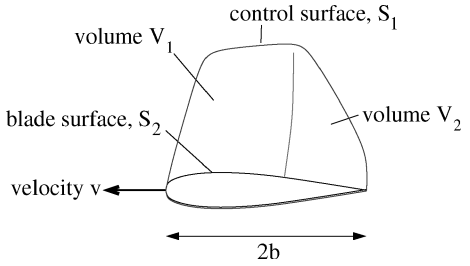

Fig. 16 Surfaces and volumes used in modeling.

independent of spatial coordinate. The v_i in the second term on the right-hand side can be taken inside the derivative, and the last two volume integrals can be replaced by surface integrals using Gauss's theorem. Because there will be no flowfield fluctuations an infinite distance from the surfaces, these are zero and Eq. (27) becomes

$$\int_{S_1} \rho_0 u_n + \rho'(u_n - v_n)\,\mathrm{d}S = \int_{V_\infty} \frac{\mathrm{D}_v\overline{\rho'}}{\mathrm{D}t}\,\mathrm{d}V \tag{28}$$

Writing the generalized density as $\overline{\rho'} = \rho' H(f)$, it follows that the convective derivative can be expressed as

$$\frac{\mathrm{D}_v\overline{\rho'}}{\mathrm{D}t} = H(f)\frac{\mathrm{D}_v\rho'}{Dt} + \rho'\frac{\mathrm{D}_v H(f)}{\mathrm{D}t} = H(f)\frac{\mathrm{D}_v\rho'}{\mathrm{D}t}$$

Substituting into Eq. (28) and denoting the volume outside of the control surface S_1 by V_{OS1} gives

$$\int_{S_1} \rho_0 u_n + \rho'(u_n - v_n)\,\mathrm{d}S = \int_{V_\infty} H(f)\frac{\mathrm{D}_v\rho'}{\mathrm{D}t}\,\mathrm{d}V = \int_{V_{OS1}} \frac{\mathrm{D}_v\rho'}{\mathrm{D}t}\,\mathrm{d}V \tag{29}$$

The same procedure can then be performed with generalized variables defined with respect to the blade surface S_2, rather than the control surface S_1. Using the fact that $u_n = v_n$ on S_2 and denoting the volume outside of S_2 by V_{OS2} gives

$$\int_{S_2} \rho_0 v_n\,\mathrm{d}S = \int_{V_{OS2}} \frac{D_v\rho'}{\mathrm{D}t}\,\mathrm{d}V \tag{30}$$

Both sides of this integral must be zero because ρ_0 and $\boldsymbol{v}$ do not vary. Combining Eqs. (29) and (30) gives

$$\int_{S_1} \rho_0 u_n + \rho'(u_n - v_n)\,\mathrm{d}S = -\int_{V_{OS2}-V_{OS1}} \frac{\mathrm{D}_v\rho'}{\mathrm{D}t}\,\mathrm{d}V \tag{31}$$

The left-hand side of this equation is the integral over the permeable control surface $I_1(t) = \int_{S_1} \rho_0 U_n\,\mathrm{d}S$, whereas $V_{OS2} - V_{OS1}$ is the volume enclosed between the blade and the control surface. This equation, therefore, relates the acoustic source integral to flow quantities in the enclosed volume. It is exact for a fixed blade pitch angle; no modeling approximations have yet been made.

It is now assumed that, in the region between the blade and control surfaces, the density is uniform either side of the shock and undergoes a step change across it, as shown diagrammatically in Fig. 17.

When the step change is expressed mathematically, the expressions for the density and its convective derivative become

$$\rho = \rho_1 1 - Hx - x_s(t) + \rho_2 Hx - x_s(t) \tag{32}$$

$$\begin{aligned}\frac{\mathrm{D}_v\rho}{\mathrm{D}t} &= \frac{\mathrm{D}_v\rho_1}{\mathrm{D}t}1 - Hx - x_s(t) + \frac{\mathrm{D}_v\rho_2}{\mathrm{D}t}Hx - x_s(t) \\ &\quad + (\rho_2 - \rho_1)\frac{\mathrm{D}_v Hx - x_s(t)}{\mathrm{D}t} \\ &= \frac{\mathrm{D}_v\rho_1}{\mathrm{D}t}1 - Hx - x_s(t) + \frac{\mathrm{D}_v\rho_2}{\mathrm{D}t}Hx \\ &\quad - x_s(t) - (\rho_2 - \rho_1)\frac{\mathrm{D}_v x_s}{\mathrm{D}t}\delta x - x_s(t)\end{aligned} \tag{33}$$

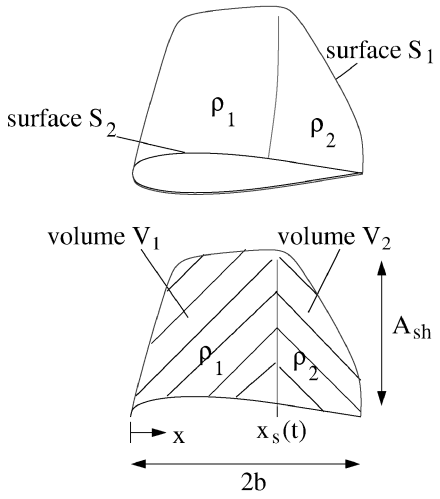

Fig. 17 Modeling the spatial density variation.

Substituting into Eq. (31) (because $\mathrm{D}_v\rho'/\mathrm{D}t = \mathrm{D}_v\rho/\mathrm{D}t$) gives

$$\begin{aligned}\int_{S_1} \rho_0 u_n + \rho'(u_n - v_n)\,\mathrm{d}S &= -\int_{V_1} \frac{\mathrm{D}_v\rho_1}{\mathrm{D}t}\,\mathrm{d}V - \int_{V_2} \frac{\mathrm{D}_v\rho_2}{\mathrm{D}t}\,\mathrm{d}V \\ &\quad + \int_{V_{OS2}-V_{OS1}} (\rho_2 - \rho_1)\frac{\mathrm{D}_v x_s}{\mathrm{D}t}\delta x - x_s(t)\,\mathrm{d}V\end{aligned} \tag{34}$$

The first two integrals become volume multiplications because their integrands do not vary spatially. The third integral can be reduced to an area integral by integration over the delta function, and if it is then assumed that the shock area per unit length, A_{sh}, does not vary significantly throughout the shock motion, this becomes an area multiplication,

$$\begin{aligned}\int_{S_1} \rho_0 u_n + \rho'(u_n - v_n)\,\mathrm{d}S &= -\frac{\mathrm{D}_v\rho_1}{\mathrm{D}t}V_1 - \frac{\mathrm{D}_v\rho_2}{\mathrm{D}t}V_2 \\ &\quad + (\rho_2 - \rho_1)\frac{\mathrm{D}_v x_s}{\mathrm{D}t}A_{\mathrm{sh}}\end{aligned} \tag{35}$$

By representing the shock position as the sum of a mean and fluctuating part, $x_s = \overline{x_s} + x_s'$, it is seen that for the shock area per unit length to be approximately constant, the fluctuating part of the shock position must be sufficiently small. This is consistent with the system identification assumption of dynamic linearity. Under this assumption, the volumes V_1 and V_2 can be expressed as $V_1 = \overline{V_1} + A_{\mathrm{sh}}x_s'$ and $V_2 = \overline{V_2} - A_{\mathrm{sh}}x_s'$, and by considering the fluctuating part of Eq. (35), an equation relating the fluctuating component of the integral, $I_1'(t)$, to the fluctuating part of the shock position x_s' is obtained.

$$I_1'(t) = A_{\mathrm{sh}}x_s'\left(\frac{\mathrm{D}_v\rho_2}{\mathrm{D}t} - \frac{\mathrm{D}_v\rho_1}{\mathrm{D}t}\right) + (\rho_2 - \rho_1)\frac{\mathrm{D}_v x_s'}{\mathrm{D}t}A_{\mathrm{sh}} \tag{36}$$

Because the mean values of the density derivatives are zero, linearizing gives

$$I_1'(t) = (\bar{\rho}_2 - \bar{\rho}_1)\frac{\mathrm{D}_v x_s'}{\mathrm{D}t}A_{\mathrm{sh}} \tag{37}$$

Taking Laplace transforms and setting $s = i\omega$ finally leads to the transfer function,

$$I_1(\omega)/x_s(\omega) = A_{\mathrm{sh}}(\bar{\rho}_2 - \bar{\rho}_1)i\omega \tag{38}$$

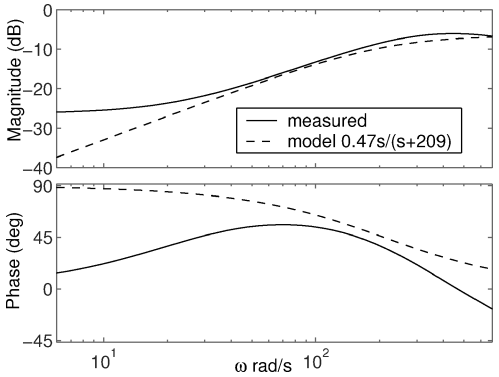

a) Blade speed to integral of $\rho_0 U_n$

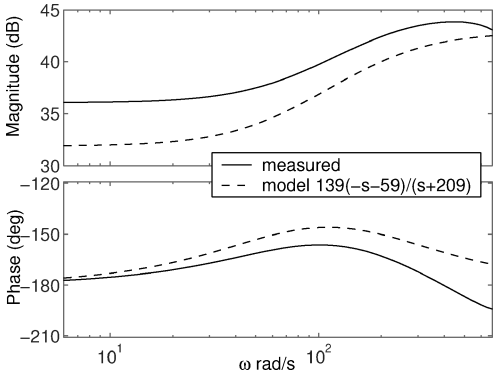

b) Blade speed to integral of L_x

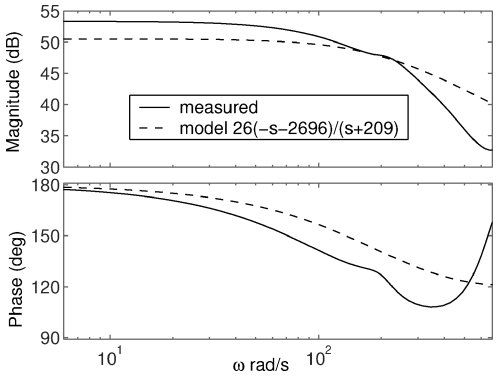

c) Blade speed to integral of L_y

Fig. 18 Comparison of the frequency responses predicted by the modeling to the measured ones.

It is apparent that the dynamics of the acoustic source integral depend on the derivative of the shock position fluctuation (the shock speed).

To derive similar approximate relations for $I_2(t) = \int_{S_1} L_x \, \mathrm{d}S$ and $I_3(t) = \int_{S_1} L_y \, \mathrm{d}S$, the momentum equation, valid for all space, is considered with generalized variables defined with respect to the control surface and the blade surface in turn. It is assumed that the shock height is approximately constant, that the variables ρu_x and ρu_y are uniform within the volumes V_1 and V_2 and undergo a step change across the shock, and that the blade upper surface pressure p_b and its component in the x direction, $p_b n_x$, are uniform either side of the shock and undergo a step change across it. The resulting equations are linearized to yield the following transfer functions:

$$\frac{I_2(\omega)}{x_s(\omega)} = A_{\mathrm{sh}}\left(((\overline{\rho u_x})_2 - (\overline{\rho u_x})_1)i\omega - \frac{(\overline{p_b n_x})_2 - (\overline{p_b n_x})_1}{A_{\mathrm{sh}}}\right) \quad (39)$$

$$\frac{I_3(\omega)}{x_s(\omega)} = A_{\mathrm{sh}}\left(((\overline{\rho u_y})_2 - (\overline{\rho u_y})_1)i\omega - \frac{\bar{p}_{b2} - \bar{p}_{b1}}{A_{\mathrm{sh}}}\right) \quad (40)$$

The dynamics of these acoustic source integrals depend on both the shock position and velocity, and as such their frequency responses will involve an extra changeover frequency compared to the shock position dynamics.

To obtain an idea of the validity of the modeling, a test case was considered in which the blade speed varied with a sum of sines form about a mean of 262.2 ms^{-1} for a fixed pitch angle of 3.66 deg. From the CFD simulation, the average values of the discontinuities across the shock were seen to be

$$A_{\mathrm{sh}} = 0.85 \text{ m}, \qquad \bar{\rho}_2 - \bar{\rho}_1 = 0.44 \text{ kgm}^{-3}$$

$$(\overline{\rho u_x})_2 - (\overline{\rho u_x})_1 = -130 \text{ kgm}^{-2} \text{ s}^{-1}$$

$$(\overline{\rho u_y})_2 - (\overline{\rho u_y})_1 = -24 \text{ kgm}^{-2} \text{ s}^{-1}$$

$$\bar{p}_{b2} - \bar{p}_{b1} = 5.5 \times 10^4 \text{ Pa}, \qquad (\overline{p_b n_x})_2 - (\overline{p_b n_x})_1 = 6500 \text{ Pa}$$

Substituting these values into Eqs. (38–40) and combining with the transfer function from blade speed fluctuation to shock position (node) fluctuation in Eq. (7) (where $i_s = x_s/138$), the following approximate transfer functions from blade speed fluctuation to acoustic source integral fluctuations are obtained.

$$\frac{I_1(\omega)}{v(\omega)} = \frac{0.47i\omega}{i\omega + 209} \quad (41)$$

$$\frac{I_2(\omega)}{v(\omega)} = \frac{139(-i\omega - 59)}{i\omega + 209} \quad (42)$$

$$\frac{I_3(\omega)}{v(\omega)} = \frac{26(-i\omega - 2696)}{i\omega + 209} \quad (43)$$

The frequency responses of these approximate transfer functions are compared to the actual responses in Fig. 18. The agreement is reasonably good; the general shapes of both the magnitude and phase variations with frequency are captured well, although there are slight differences in the exact levels.

This agreement confirms that the dynamics of the acoustic source integrals are caused primarily by the unsteadiness of the shock, as expected from previous work suggesting that significant noise originates at the shock surfaces at transonic speeds.

Conclusions

The permeable surface form of the FW–H equation provides an efficient basis for noise prediction at transonic speeds and requires knowledge of the temporal variation of fictitious acoustic sources on the permeable control surface. In response to the fact that performing full unsteady CFD calculations for maneuvering helicopters will be too time consuming for use in design, the potential for using low-order modeling as an efficient alternative has been considered.

Because it is known for transonic flows that much of the noise originates at the shock surfaces, the dynamics of the shock position was first considered to provide an insight. Two-dimensional CFD simulations were performed in which the blade speed and blade pitch angle variations were varied harmonically. The response of the shock position was seen to exhibit a frequency-dependent phase lag or time delay with respect to the blade speed and pitch angle variations.

System identification was then used to obtain low-order models for the response of the shock position. The model structures were based on IIR filters, and the input blade speed/blade pitch angle variations were chosen to contain a wide range of frequencies without suffering from noise or nonlinearity limitations. Low-order models describing the transfer functions from blade speed/blade pitch angle variations to shock position variation were obtained; both were seen to have the approximate form of first-order lags and were consistent with the phase lags observed for harmonic forcing.

To avoid the complexity of considering the acoustic sources at all points on the control surface, two-dimensional flow in which the section of the control surface was acoustically compact was considered. In such flow, the integrals of the acoustic sources over

the control surface contour provide sufficient information for sound prediction. The same system identification techniques were used to obtain low-order models for the transfer functions from the blade speed/blade pitch angle variations to the variations in the acoustic source integrals. These models were successfully used in noise prediction. An analytical consideration of the acoustic source integrals strongly suggested that their main unsteadiness was caused by the dynamics of the shock.

Thus, the potential for using low-order modeling for the acoustic sources has been demonstrated in two dimensions. The techniques are extendable to three-dimensional problems, although the computational times involves in obtaining models for the acoustic sources would be significantly increased.

Acknowledgments

The authors thank the Engineering and Physical Sciences Research Council, Westland Helicopters, Ltd., and Thales Underwater Systems, Ltd., for their financial support. They are grateful to T. P. Hynes and S. A. Karabasov for making their computational fluid dynamics code readily available.

References

[1]Ffowcs Williams, J. E., and Hawkings, D. L., "Sound Generation by Turbulence and Surfaces in Arbitrary Motion," *Philosophical Transactions of the Royal Society*, Vol. A264, May 1969, pp. 321–342.

[2]Morgans, A. S., and Dowling, A. P., "The Aeroacoustics of Transonic Helicopter Blades," AIAA Paper 2002-2545, June 2002.

[3]di Francescantonio, P., "A New Boundary Integral Formulation for the Prediction of Sound Radiation," *Journal of Sound and Vibration*, Vol. 202, No. 4, 1997, pp. 491–509.

[4]Brentner, K. S., and Farassat, F., "Analytical Comparison of the Acoustic Analogy and Kirchhoff Formulation for Moving Surfaces," *AIAA Journal*, Vol. 36, No. 8, 1998, pp. 1379–1386.

[5]Hanson, D. B., and Fink, M. R., "The Importance of Quadrupole Sources in Prediction of Transonic Tip Speed Propeller Noise," *Journal of Sound and Vibration*, Vol. 62, No. 1, 1979, pp. 19–38.

[6]Farassat, F., and Tadghighi, H., "Can Shock Waves on Helicopter Rotors Generate Noise? A Study of the Quadrupole Source," *Annual Forum Proceedings, American Helicopter Society*, Vol. 1, American Helicopter Society, Alexandria, VA, 1990, pp. 323–346.

[7]Schmitz, F. H., and Yu, Y. H., "Helicopter Impulsive Noise: Theoretical and Experimental Status," *Journal of Sound and Vibration*, Vol. 109, No. 3, 1986, pp. 361–427.

[8]Farassat, F., "Linear Acoustic Formulas for Calculation of Rotating Blade Noise," *AIAA Journal*, Vol. 19, No. 9, 1981, pp. 1122–1130.

[9]Brentner, K. S., and Lyrintzis, A. S., and Koutsavdis, E. K., "Comparison of Computational Aeroacoustic Prediction Methods for Transonic Rotor Noise," *Journal of Aircraft*, Vol. 34, No. 4, 1997, pp. 531–538.

[10]Beddoes, T. S., "Two and Three Dimensional Indicial Methods for Rotor Dynamic Airloads," American Helicopter Society Specialist's Meeting on Rotorcraft Dynamics, American Helicopter Society, Alexandria, VA, 1989.

[11]Leishman, J. G., "Subsonic Unsteady Aerodynamics Caused by Gusts Using the Indicial Method," *Journal of Aircraft*, Vol. 33, No. 5, 1996, pp. 869–879.

[12]Leishman, J. G., "Aeroacoustics of 2-D and 3-D Blade Vortex Interaction Using the Indicial Method," *American Helicopter Society 52nd Annual Forum*, American Helicopter Society, Alexandria, VA, 1996.

[13]Dowell, E. H., Hall, K. C., and Romanowski, M. C., "Reduced Order Aerodynamic Modeling of How to Make CFD Useful to an Aeroelastician," ASME Aerospace Div., Vol. 53-3, No. 149–163, American Society of Mechanical Engineers, Fairfield, NJ, 1997.

[14]Dowell, E. H., Hall, K. C., Thomas, J. P., Florea, R., Epureanu, B. I., and Heeg, J., "Reduced Order Models in Unsteady Aerodynamics," *AIAA/ASME/ASCE/AHS/ASC Structures, Structural Dynamics, and Materials Conference*, Vol. 1, AIAA, Reston, VA, 1999, pp. 622–637.

[15]Raveh, D. E., "Reduced Order Models for Nonlinear Unsteady Aerodynamics," *AIAA Journal*, Vol. 39, No. 8, 2001, pp. 1417–1429.

[16]Ballaus, W. F., "Some Recent Progress in Transonic Flow Computations," *Numerical Methods in Fluid Dynamics*, Hemisphere, New York, 1978, Chap. 3, pp. 155–235.

[17]Ljung, L., *System Identification: Theory for the User*, Prentice–Hall, Upper Saddle River, NJ, 1999.

[18]Soderstrom, T., and Stoica, P., *System Identification*, Prentice–Hall, Upper Saddle River, NJ, 1989.

[19]Ballaus, W. F., and Goorjian, P. M., "Computation of Unsteady Transonic Flows by Indicial Methods," *AIAA Journal*, Vol. 16, No. 2, 1978, pp. 117–124.

[20]Cowan, T. J., Arena, A. S. Jr., and Gupta, K. K., "Accelerating Computational Fluid Dynamics Based Aeroelastic Predictions Using System Identification," *Journal of Aircraft*, Vol. 38, No. 1, 2001, pp. 81–87.

[21]Zhu, M., and Dowling, A. P., and Bray, K. N. C., "Flame Transfer Function Calculations for Combustion Oscillations," American Society of Mechanical Engineers, ASME Paper 2001-FT-374, June 2001.

[22]Tadghighi, H., Holz, R., Farassat, F., and Lee, Y. J., "Development of a Shock Noise Prediction Code for High Speed Helicopters—The Subsonically Moving Shock," *American Helicopter Society 47th Annual Forum*, American Helicopter Society, Alexandria, VA, 1991.

[23]Tijdeman, H., and Seebass, R., "Transonic Flow past Oscillating Airfoils," *Annual Review of Fluid Mechanics*, Vol. 2, 1980, pp. 181–222.

[24]Rusak, Z., Giddings, T. E., and Cole, J. D., "Interaction of a Weak Shock with Freestream Disturbances," *AIAA Journal*, Vol. 33, No. 6, 1995, pp. 977–984.

[25]McCroskey, W. J., "The Effects of Gusts on the Fluctuating Airloads of Airfoils in Transonic Flow," *Journal of Aircraft*, Vol. 22, No. 3, 1985, pp. 236–243.

[26]Plotkin, K. J., "Shock Wave Oscillation Driven by Turbulent Boundary-Layer Fluctuations," *AIAA Journal*, Vol. 13, No. 8, 1975, pp. 1036–1040.

[27]Karabasov, S. A., and Hynes, T. P., "Open Boundary Conditions of Predictor-Corrector Type for External Flows," AIAA Paper 2002-2442, June 2002.

[28]Ljung, L., *System Identification Toolbox User's Guide*, Mathworks, Natick, MA, 1991.

W. Ng
Associate Editor